Supplemental Document

optica

Interference-enhanced chirality-reversible dichroism metalens imaging using nested dual helical surfaces: supplement

CHENQIAN WANG[1,2] AND CHINHUA WANG[1,2,*]

[1] *School of Optoelectronics Science and Engineering and Collaborative Innovation Center of Suzhou Nano Science and Technology,Soochow University, Suzhou 215006, China*
[2] *Key Lab of Advanced Optical Manufacturing Technologies of Jiangsu Province and Key Lab of Modern Optical Technologies of Education Ministry of China, Soochow University, Suzhou 215006, China*
[*] *Corresponding author: chinhua.wang@suda.edu.cn*

This supplement published with The Optical Society on 8 April 2021 by The Authors under the terms of the Creative Commons Attribution 4.0 License in the format provided by the authors and unedited. Further distribution of this work must maintain attribution to the author(s) and the published article's title, journal citation, and DOI.

Supplement DOI: https://doi.org/10.6084/m9.figshare.14182442

Parent Article DOI: https://doi.org/10.1364/OPTICA.418128

Interference-Enhanced Chirality-Reversible Dichroism Metalens Imaging using Nested Dual Helical Surfaces

CHENQIAN WANG,[1,2] AND CHINHUA WANG[1, 2,*]

[1]*School of Optoelectronics Science and Engineering and Collaborative Innovation Center of Suzhou Nano Science and Technology, Soochow University, Suzhou 215006, China*

[2]*Key Lab of Advanced Optical Manufacturing Technologies of Jiangsu Province and Key Lab of Modern Optical Technologies of Education Ministry of China, Soochow University, Suzhou 215006, China*

**chinhua.wang@suda.edu.cn*

This document provides supplementary information to "Interference-Enhanced Chirality-Reversible Dichroism Metalens Imaging using Nested Dual Helical Surfaces".

Section 1. Bayesian optimization algorithm for acquiring the best set of parameters

For designing an optical metasurface, it is necessary to obtain the relationship between optical response and geometrical parameters of nanostructure in micro-nanometer scale. Calculation amount for conventional grid search method is exponentially increase for structure/model characterized with multi-parameters. Bayesian optimization is a convenient and economical way for this calculation.

Fig. S1 shows the schematic diagram of Bayesian optimization in our calculation. A number of points was chosen as initial points in random in the full parameter hyperspace (each parameter is a dimension and often need to be limited with boundaries and normalized) and sent to FDTD for calculation. The calculation process in FDTD was considered as a black box function (objective function) which inputs a set of parameters and outputs optical responses. In this work, some parameters were associated with each other to reduce the amount of calculation (period P = 2×outer radius R_2, outer radius R_2 = 2×inner radius R_1, outer height H_2 = inner height H_1), and cross-polarization transmittivity (T_{LR}) was chosen as target function for optimization, in which a prior function of Gaussian process is used to establish a regression model from separate points. Subsequent group of parameters was selected by acquisition function (in this work, acquisition function is upper confidence bound, UCB), from which the calculation result was used to amend the original regression model if the requirement of optimization is not satisfied. From the Bayesian optimization, a set of optimized group of parameters can be obtained.

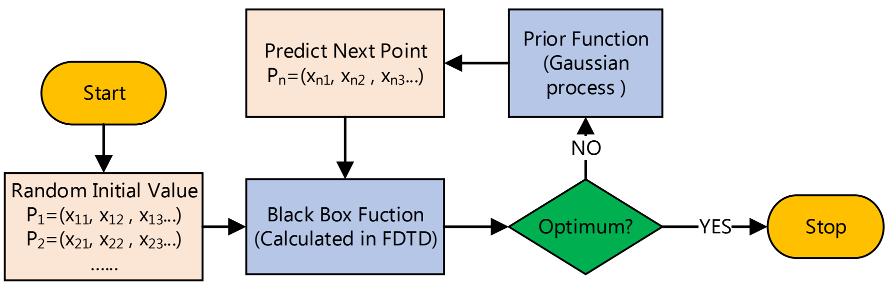

Figure S1. Flow chart of Bayesian optimization in calculation.

Section 2. Dependences of the co-polarization components in transmission on azimuthal angles in a NDHS

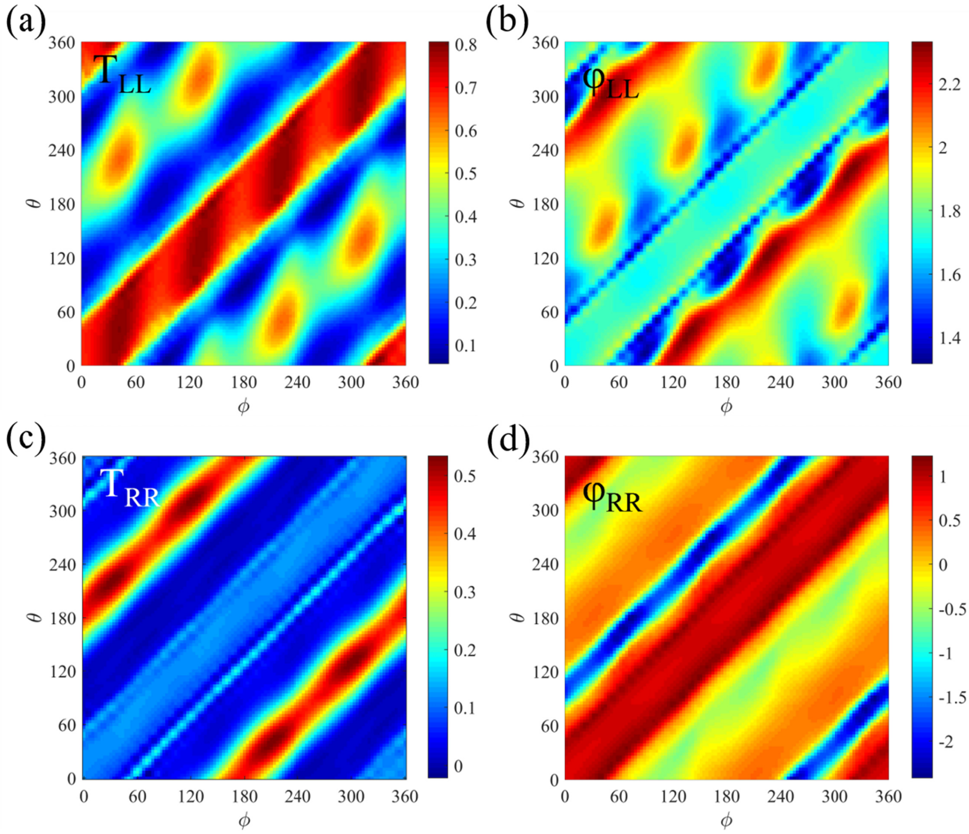

Fig. S2. (a) Transmissivity and (b) Phase shift of co-polarization component for LCP incidence as a function of azimuthal angle θ and ϕ. (c) Transmissivity and (d) Phase shift of co-polarization component for RCP incidence as a function of azimuthal angle θ and ϕ.

Section 3. Electric fields at different heights in the NDHS structure with different twist angles

Figure S3 shows the electric fields at different heights in the NDHS structure with different twist angles of Ψ=0°(**1st** row), 75°(**2nd** row) and 140°(**3rd** row), respectively, in the case of LCP incidence on a left-handed surface. It is seen that strong field enhancement occurs between IHS and OHS in the case of optimized Ψ=75°[in the band of (60°, 100°)], in which strong interference field remains in the gap between IHS and OHS at four different heights (Z = 0.25, 0.5, 0.75 and 1 μm) while no interaction between IHS and OTS can be observed in other twist angles, such as 0° and 140°, which is consistent with that observed in Fig. 3.

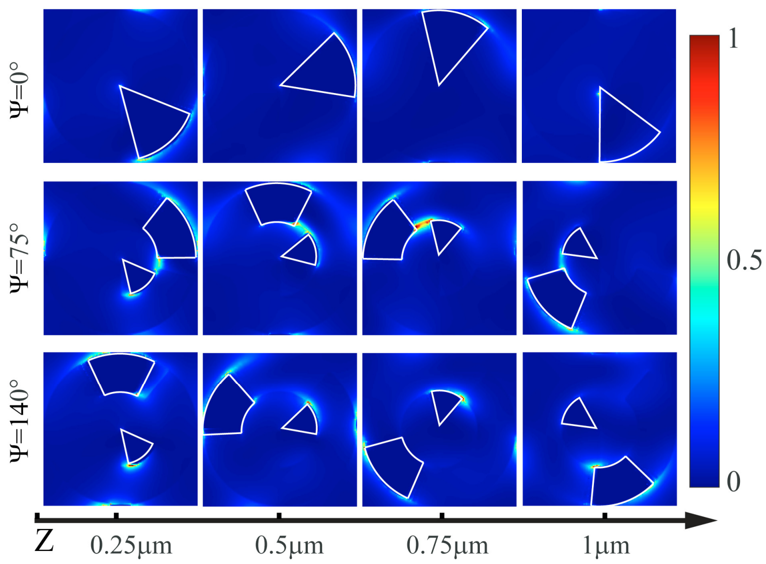

Fig. S3. Electric fields at different heights in NDHS structure with different twist angles in the case of LCP incidence on a left-handed surface.

Section 4. Enhancement of cross polarization conversion in the case of RCP incidence on left-handed NDHS surface

The interaction between IHS and OHS in the case of RCP incidence on left-handed NDHS surface can be written based on the theory in main text with minor changes:

$$\begin{aligned} \mathrm{E}_{\mathrm{RL}} &\propto t_{1\mathrm{RL}} E_i e^{i\Phi_1} + t_{2\mathrm{RL}} E_i e^{i(\Phi_2 - 2\Psi)} \\ \mathrm{E}_{\mathrm{RR}} &\propto t_{3\mathrm{RR}} E_i e^{i\Phi_3} + t_{4\mathrm{RR}} E_i e^{i(\Phi_4 - 2\Psi)} \end{aligned} \tag{S1}$$

Where ERL and ERR are the LCP (i.e., cross-polarized) and RCP (i.e., co-polarized) components in the transmitted electric field with a RCP incidence. t_{1RL}, t_{2RL} and t_{3RR}, t_{4RR} are the transmission coefficient of cross-polarization and co-polarization transmission component of the IHS and OHS, respectively. Φ_1, Φ_2 and Φ_3, Φ_4 are the corresponding phase shifts of the cross-polarization and co-polarization component. Ψ is the twist angle between the IHS and OHS. Similarly, To maximize the cross-polarization component, the condition of constructive interference between IHS and OHS must be satisfied, i.e.,

$$\Phi_1 - \Phi_2 + 2\psi = 2n\pi \tag{S2}$$

Therefore, Ψ is around 60° when n=0, which is consistent with line 1 in Fig. 3(d), and Ψ is around 120° when n=1, which is consistent with line 2 in Fig. 3(d).

Section 5. Quantitative evaluation of the fabrication errors and their impact on device performance

In the fabrication of 3D structure using direct laser writing system, the moving path of the laser beam or the sample platform is programmed based on the designed pattern. The theoretical pattern after two-photon polymerization should be a dot (single shot) or a line (writing along a line). However, the practical pattern after writing is usually an ellipsoid or a cylinder (with a radius) in reality. The schematic of the moving path in fabrication is shown in Fig. S4(a). To show the difference between the theoretical design and practical fabrication, a relationship between ***LaserPower*** (a parameter related/proportional to laser power in direct laser writing system, which is unitless) and radius of the cylinder was experimentally established, which is shown in Fig. S4(b). It is seen from Fig. S4(b) that the relationship is approximately linear when ***LaserPower*** is larger than 33 while no patterns can be formed if the ***LaserPower*** is smaller than 33 because energy is below the threshould of two-photon polymerization. The errorbars in Fig. S4(b) indicate the standard deviation from measurements for each cylinder across five different locations, which is within 30 nm at different laser powers.

Based on the two-photon polymerization, arbitrary 3D structures can be constructed by scanning the laser beam or the sample platform. From Fig. S4(b), it is also seen that the lower the laser power, the higher the structural precision. However, lower ***LaserPower*** means more writting paths and longer writting time.

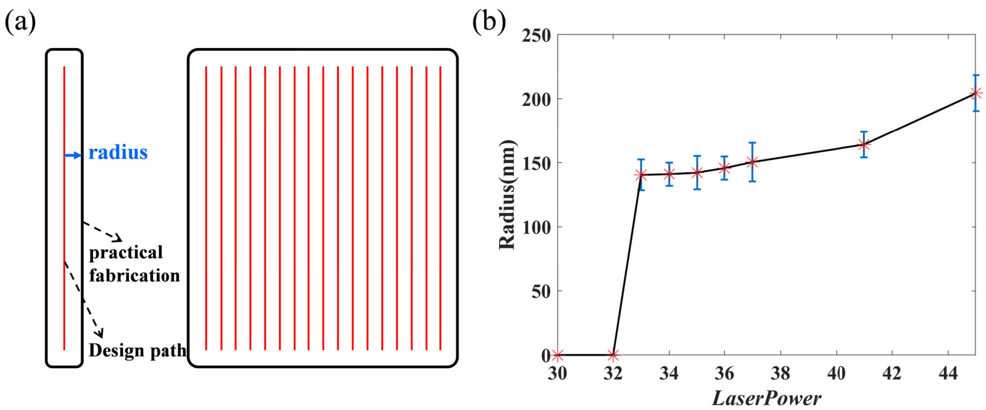

Figure S4. (a) Schematics for design and practical fabrication. Red Line: design path; black box: practical fabrication results. (b) Relationship between ***LaserPower*** setting and radius of cylinder in practical fabrication.

The fabrication errors or deviations of the structural parameters on the performance of the device are performed based on the Bayesian optimization algorithm shown in **Supplement 1 Section 1**. Massive calculated results indicate that our design has a high tolerance in parameter range. Detailed calculation shows that the tolerance range for parameters P ($P = 2\times R_2$, $R_2 = 2\times R_1$), H_1 (H_2), d, and Ψ are 1900 nm to 2120 nm, 1200 nm to 1630 nm, 120 nm to 220 nm and 65° to 85°, respectively, if the overall cross-polarization conversion efficiency of the metalens is decreased by 5% from the best optimized value. This tolerance can be well achieved with the proposed two-photon polymerization method.

Section 6. Additional schematics of optical imaging and measurement system

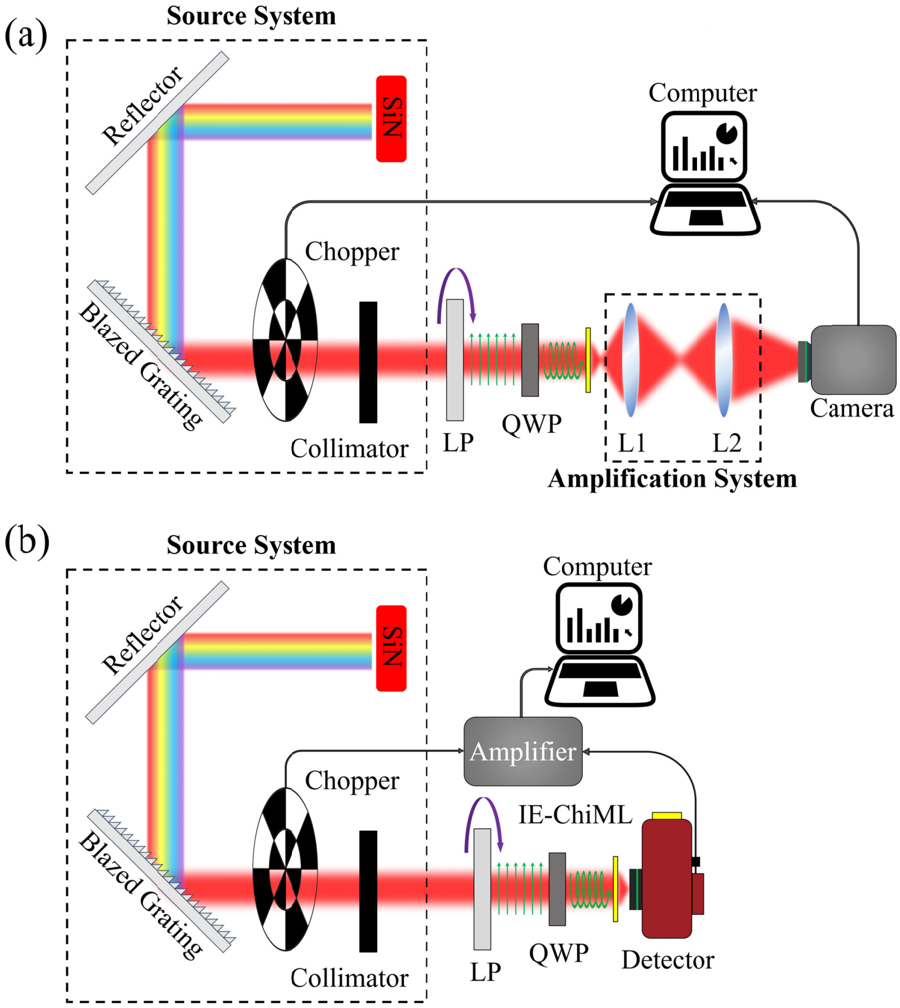

Figure S5. Schematics of the optical imaging and measurement system. (a) focusing measurement. (b) Circular polarization dichroism measurement. SiN: silicon nitride infrared source; LP: linear polarizer; QWP: quarter-wave plate; L1: lens 1; L2: lens 2; L3: lens 3; Amplifier: Lock-in Amplifier (Stanford SR830); Detector: HgCdTe detector (EG&G Judson).

Section 7. Details about lock-in imaging technique

Because of intense background infrared radiation in the infrared wavelength range of interests, lock-in technique was utilized to extract effective signal from the environment noise. Input signal (S_i) and reference signal (S_r) with same frequency f_{in} are

$$\begin{aligned} S_i &= A_i \sin(2\pi f_{\mathrm{in}} t + \varphi_i) + n_i(t) \\ S_r &= B_r \sin(2\pi f_{\mathrm{in}} t + \varphi_r) \end{aligned} \tag{S3}$$

where A_i and B_r are amplitude of the input signal and the reference signal, respectively. $n_i(t)$ represents the invalid signal, including noise signal and nonperiodic signal.

Input signal and reference signal were multiplied together and integrated over time for a period T

$$S_0(t) = \frac{1}{T}\int_0^T S_i(t) S_r(t) dt \tag{S4}$$

It's easy to show the results of time integral for noise and nonperiodic part are zero. Thus, only the signal with frequency f_{in} can be measured so that the noise eliminating is achieved.

In our experiment, a set of time sequentially sampled images (1000 photos) with an acquisition frequency of 100 Hz are taken by thermal imaging camera. These images were tailored to square array (512×512 pixels) for reducing the amount of calculation. Each pixel in these photos is an independent channel (total 512×512 channels) and undergoes in parallel phase lock-in processing (based on Eq. S4) using Matlab (*Matlab*, Mathworks). The results of intensity S_0 of valid signal in each pixel are recombined into a full image (512×512 pixels), i.e., images after lock-in process.